Earth and Planetary Science Letters 613 (2023) 118171

Contents lists available at ScienceDirect

Earth and Planetary Science Letters

journal homepage: www.elsevier.com/locate/epsl

Calcium isotope constraints on the origin of eucrites and diogenites: The role of magma ocean and magmatism

Yongli Xue [a,b], Jinting Kang [b,c,d,*], Shiyong Liao [e,d], Runlian Pang [f], Huimin Yu [b,c,d], Zifu Zhao [b,c,d], Zhaofeng Zhang [g], Bingkui Miao [h], Weibiao Hsu [e,c,d], Fang Huang [b,c,d]

[a] Key Laboratory of Gemological Design and Testing, School of Jewelry and Art Design, Wuzhou University, Wuzhou, 543002, China
[b] CAS Key Laboratory of Crust-Mantle Materials and Environments, School of Earth and Space Sciences, University of Science and Technology of China, Hefei 230026, China
[c] Deep Space Exploration Laboratory, University of Science and Technology of China, Hefei 230026, China
[d] CAS Center for Excellence in Comparative Planetology, USTC, Hefei 230026, Anhui, China
[e] Purple Mountain Observatory, Chinese Academy of Sciences, Nanjing 210023, China
[f] State Key Laboratory of Ore Deposit Geochemistry, Institute of Geochemistry, Chinese Academy of Sciences, Guiyang, 550081, China
[g] Research Center for Planetary Science, Chengdu University of Technology, Chengdu, 610059, China
[h] Institution of Meteorites and Planetary Materials Research, Key Laboratory of Planetary Geological Evolution, Guilin University of Technology, Guilin 541006, China

ARTICLE INFO

Article history:
Received 1 October 2022
Received in revised form 7 April 2023
Accepted 12 April 2023
Available online 4 May 2023
Editor: J. Badro

Keywords:
Ca isotopes
eucrite
diogenite
Vesta
achondrite

ABSTRACT

Howardite-Eucrite-Diogenite (HED) meteorites represent a large suit of crustal and sub-crustal rocks from the Vesta. This work presents systematic examination of the Ca isotope data on multiple varieties of HED meteorites for a better understanding of the magmatic evolution of the Vesta. Falls and finds possess similar Ca isotope compositions, and no correlation is observed between $\delta^{44/40}$Ca and $(Sr/Eu^*)_n$, indicating that terrestrial weathering effect on Ca isotopes is insubstantial. According to the data in literature, the inner solar system may have a homogeneous $\delta^{44/40}$Ca and the average of inner solar system bodies (0.97 ± 0.03‰) can approximate the composition of bulk silicate Vesta (BSV). Basaltic eucrites define a cluster in $\delta^{44/40}$Ca (0.95 ± 0.07‰, 2SD, N = 15) that is higher than the terrestrial mid-ocean ridge basalts (~0.85‰). Combined with partial melting and magma ocean differentiation modeling, the Ca isotope signatures suggest that eucrites represent the residual melts evolved from a magma ocean formed by primordial Vesta's moderate-to-high degree melting (20-100%). Diogenites have distinguishingly higher $\delta^{44/40}$Ca (1.18 ± 0.15‰, 2SD, N = 7) than the basaltic eucrites, which displays a negative correlation with the $1000 \times$ Lu/Ti ratio and a positive correlation with 1/Ca. However, magma ocean crystallization can only explain diogenites with $\delta^{44/40}$Ca higher than 1.17‰, suggesting that diogenites have complicated petrogenesis and are not necessarily cogenetic with eucrites. Diogenites with $\delta^{44/40}$Ca < 1.17‰ may result from magma-ocean-cumulate partial melts intruding the eucritic crust. Mixing models suggest that the eucritic component in these diogenites may be less than 10%. Two howardites have lower $\delta^{44/40}$Ca of 0.80 ± 0.04‰ and 0.86 ± 0.05‰ than eucrites and diogenites. This signature may reflect the addition of carbonaceous chondritic materials due to impact brecciation.

1. Introduction

The primordial characteristics of the planets were molded by early solar system magmatism, but most rock records have been lost due to protracted geological activity. Achondrite, which represents magmatic remnants in different stages of planetary evolution (from asteroids to differentiated planets), can preserve information about the early solar system. The howardite-eucrite-diogenite (HED) clan of meteorites is the most common achondrite in the global meteorite collection. Eucrites have a chemical composition like basalt and their magmatic textures suggest a volcanic or intrusion formation, referring to basaltic eucrites and cumulate eucrites, respectively. Diogenites are mostly coarser-grained orthopyroxenites and howardites are polymict breccias comprised of both eucritic and diogenitic clasts. The similar chemistry and mineralogy between the HED clan and 4-Vesta were revealed by remote sensing spectroscopy (e.g., Gaffey et al., 1989) and visible and infrared

* Corresponding author at: School of Earth and Space Sciences, University of Science and Technology of China, Hefei 230026, China.
E-mail address: kjt@ustc.edu.cn (J. Kang).

https://doi.org/10.1016/j.epsl.2023.118171
0012-821X/

spectroscopy by the Dawn spacecraft (e.g., Russell et al., 2012), indicating that HEDs are samples from the Vestan crust. Therefore, HED meteorites provide a valuable opportunity to study the early evolution of a differentiated planetesimal through a combination of geochemical analyses of meteorites, remote sensing, and spectroscopic studies of the planetary surface.

Although HED meteorites have been extensively studied for petrology and mineralogy over the past fifty years, their petrogenesis is still enigmatic. Two models have been proposed for the origin of eucrites and diogenites. First, eucrites and diogenites may result from partial melting of a primitive asteroid, with the eucritic magma extracted to the surface and leaving behind an olivine-rich residual mantle (e.g., Stolper, 1977). Alternatively, the radioactive decay of short-lived isotopes such as ^{26}Al and ^{60}Fe may have caused global melting on early Vesta and formed a deep magma ocean (Greenwood et al., 2005). Diogenites are generally thought to originate from crystals settling from the magma ocean, while eucrites represent residual liquids (e.g., Ashcroft and Wood, 2015; Righter and Drake, 1997; Ruzicka et al., 1997). Recently, many studies argued that the formation of eucrites and diogenites is more complex than previously thought, and it may involve ultramafic cumulate remelting, differentiation in discrete magma chambers, and contamination by crustal melts (e.g., Barrat et al., 2010; Mandler and Elkins-Tanton, 2013; Mitchell and Tomkins, 2019; Zhang et al., 2020).

With the advancement of isotope analytical techniques over the past two decades, the application of a range of metal-stable isotope systems sheds light on planetary accretion, differentiation, and magmatic evolution. Calcium is both a lithophile and refractory element with a 50% condensation temperature of 1517 K (Lodders, 2003), which means that Ca remains unaffected by metallic core formation or volatilization during planetary accretion (e.g., Valdes et al., 2021). Thus, the Ca isotope fractionation in differentiated asteroids is mainly controlled by magmatic processes. Terrestrial sample studies (e.g., Huang et al., 2010) and theoretical calculations (e.g., Feng et al., 2014; Wang et al., 2017) have demonstrated that olivine (Ol) and orthopyroxene (Opx) show heavier Ca isotope compositions than clinopyroxene (Cpx) and plagioclase (Plg). Melting of an Ol-rich mantle causes Ca isotope fractionation in liquids and its scale depending on the melting degree (e.g., Soderman et al., 2022). For example, melts generated by low-degree partial melting (e.g., MORB, 10-20%, Eriksen and Jacobsen, 2022) are isotopically lighter than the bulk silicate earth estimate (BSE, 0.94-1.05‰, Huang et al., 2010; Kang et al., 2017). Consequently, the Ca isotope signature in HED meteorites can provide novel insights on the magmatic evolution of Vesta.

In this study, we present high-precision Ca isotope data for fifteen eucrites, nine diogenites, and two howardites. Our new data reveal a Ca isotope dichotomy between diogenites and eucrites. Basaltic eucrites have nearly consistent Ca isotope composition with the bulk silicate Vesta (BSV), indicating a magma ocean origin. In contrast, diogenites show higher and more scattered $\delta^{44/40}$Ca, revealing that complicated magmatism occurred on Vesta.

2. Samples and methods

2.1. Sample descriptions

Twenty-six HED meteorites were analyzed in this study. Of this sample set, six samples are falls, and the remaining twenty samples are finds. In addition, two USGS terrestrial standards (BHVO-2 and PCC-1) were measured for data quality control. Eucrites are basaltic or accumulative rocks. This study includes fourteen basaltic eucrites and one cumulate eucrite. Basaltic eucrites occur as fine-grained volcanic rocks and cumulate eucrites are coarser-grained gabbros and plutonic rocks (Mittlefehldt, 2015). Diogenites are mostly coarse-grained orthopyroxenites and a small number of Ol-bearing diogenites have Ol abundance >10%. This study includes eight orthopyroxenites and one Ol-bearing sample (NWA 5480, with 30.2% Ol, Tkalcec et al., 2013).

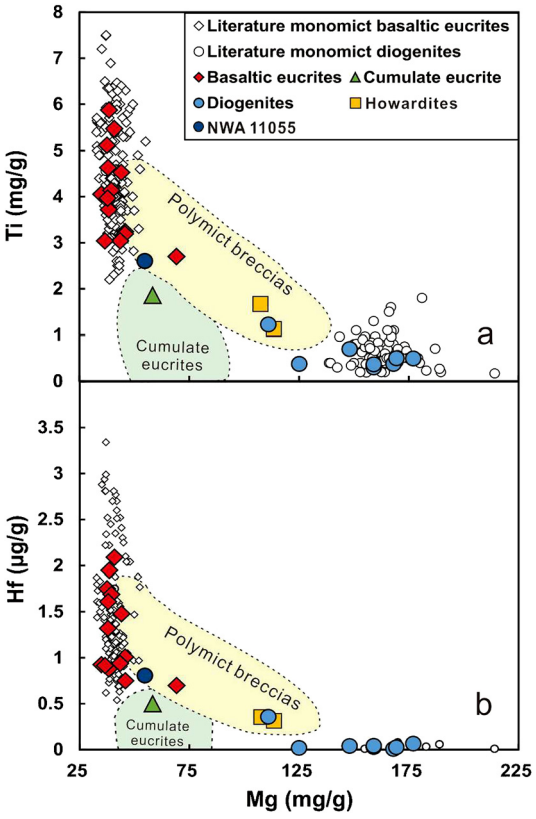

Fig. 1. (a) Ti vs. Mg and (b) Hf vs. Mg for HED meteorites showing distinct composition ranges for basaltic eucrites, diogenites, cumulate eucrite, and mixing signature of polymict breccias. Literature data of monomict basaltic eucrites and monomict diogenites are from Mittlefehldt (2015) and references therein. The field for polymict breccias and cumulate eucrites follows the ranges defined in Mittlefehldt (2015).

HED meteorites are classified into two subcategories as monomict breccias and polymict breccias. Polymict breccias are formed by impact fragmentation and are mixtures of eucritic and diogenitic clasts as well as chondritic or other exogenous clasts derived from the impactor. Conversely, monomict breccias are defined as composed of nearly 100% of single primary lithology. The polymict breccias thus form a continuum on major elemental plots from monomict basaltic eucrite to monomict diogenite breccias (Fig. 1). Howardites are typical polymict breccias that contain >10% diogenite mixed with >10% eucrite (Delaney et al., 1983). In this study, diogenites NWA 10079 and NWA 11055, eucrite NWA 11704, and howardites NWA 10695 and NWA 8362 are polymict breccias.

2.2. Analytical methods

To guarantee representative sampling, 500 mg of each meteorite was crushed and powdered into an agate mortar. About 50 mg of sample powder was weighed and fully digested by sequential mixtures of concentrated HF-HNO_3 and HNO_3-HCl. The solution was separated into two fractions for element and Ca isotope analyses, respectively. Major elements (except for Ca) and trace element compositions were analyzed by a Thermal Fisher ICP-MS X2 at Guizhou Tongwei Analytical Technology Co., Ltd. following

Table 1
Ca isotope compositions of HED meteorites.

Sample	Find/Fall	Type[a]	Mg#	CAS results				CDUT results			
				$\delta^{44/40}$Ca (‰)	2SD	2SE	n	$\delta^{44/40}$Ca (‰)	2SD	2SE	n
NWA 8336	Find	MG-NL eucrite	42.4	1.00	0.06	0.03	3				
NWA 8336-R				1.00			1				
NWA 11031	Find	MG-NL eucrite	45.4	0.89	0.01	0.01	3				
NWA 2988-R1				0.92	0.01	0.01	3				
NWA 2988-R2	Find	MG-NL eucrite	39.9	1.02	0.04	0.02	3				
NWA 2988 Average				0.97	0.04	0.03	6				
NWA 2784-1[b]				0.92	0.11	0.07	3				
NWA 2784-2[b]	Find	MG-NL eucrite	37.2	0.95	0.03	0.02	3				
NWA 2784-3[b]				0.99	0.11	0.06	3				
NWA 2784 Average				0.95	0.07	0.04	9				
Camel Donga	Find	MG-NL eucrite	38.8					0.99	0.11	0.06	3
NWA 8009	Find	MG-NL eucrite	38.9					0.88	0.07	0.04	4
NWA12570	Find	MG-NL eucrite	37.9					0.91	0.09	0.05	3
NWA12569	Find	MG-NL eucrite	38.4					0.96	0.06	0.03	3
NWA12933	Find	MG-NL eucrite	38.0					0.93	0.03	0.02	3
Millbillillie	Fall	MG-NL eucrite	43.0					0.96	0.11	0.06	3
Millbillillie-R								0.93			1
Serra Pelada	Fall	St eucrite	38.4	0.99	0.12	0.06	4				
NWA 13995	Find	St eucrite	40.0					0.94	0.06	0.03	3
NWA 13583	Find	St eucrite	40.7					0.98	0.05	0.03	3
Dhofar 007	Fall	Cumulate eucrite	51.5	1.06	0.09	0.05	3				
Tatahouine	Fall	Orthopyroxenite diogenite	77.0	1.19	0.08	0.05	3	1.23	0.07	0.04	3
Bilanga	Fall	Orthopyroxenite diogenite	80.2	1.13	0.03	0.02	3				
NWA7831	Find	Orthopyroxenite diogenite	71.2					1.09	0.05	0.03	3
NWA 14011	Find	Orthopyroxenite diogenite	72.5					1.24	0.03	0.02	3
Mazichuan	Fall	Orthopyroxenite diogenite	78.3					1.28	0.03	0.02	3
Dhofar 700	Find	Orthopyroxenite diogenite	66.8					1.22	0.05	0.03	3
Dhofar 700-R								1.22			1
NWA5480	Find	Olivine diogenite	74.6					1.10	0.03	0.02	3
NWA 11704	Find	Polymict eucrite	56.6	0.95	0.08	0.05	3				
NWA 10079	Find	Polymict diogenite	60.4	1.11	0.09	0.05	3				
NWA 10079-R				1.06			1				
NWA 11055	Find	Polymict diogenite	49.4	0.92	0.01	0.01	3				
NWA 10695	Find	Howardite	58.0	0.80	0.08	0.04	3				
NWA 8362	Find	Howardite	66.0	0.86	0.08	0.05	3				

[a] MG-NL eucrite: main group Nuevo Laredo trend eucrite; St eucrite: Stanner trend eucrite.
[b] NWA 2784-1 is from the fusion crust and show the highest degree of alteration. NWA 2784-2 is the sample between the fusion crust and the fresh core. NWA 2784-3 is from the fresh core and underwent the least alteration.

procedures in Eggins et al. (1997) with modifications as described in Li et al. (2005). The analytical precision is about 2-5%. Due to the interference of Ar and CO_2 on Ca during ICP-MS analysis, the Ca content was measured by an iCAP 7200 inductively coupled plasma-optical emission spectrometer (ICP-OES) at the University of Science and Technology of China. USGS standard W-2a was used as a reference standard and cross-checked with BHVO-2 and other reference materials.

The purification of Ca in solution follows the method described in Zhu et al. (2016). Briefly, the aliquot, which contains ~50 μg Ca, was mixed with a ^{42}Ca-^{43}Ca double spike to make an optimal $^{40}Ca_{sample}/^{42}Ca_{spike}$ of 7 and was subsequently re-dissolved in 1.6N HCl. Calcium was purified using a Teflon micro-column filled with 1 ml of AG MP-50 (100–200 mesh) resin. 6N HCl and Milli-Q water were alternately employed to clean the resin three times. 6N HCl and 8N HNO_3 were passed through the resin-filled columns to decrease the Ca blanks. The columns were then conditioned by 5 ml of 1.6N HCl. The spiked aliquot was loaded onto the column and eluted with 1.6N HCl. The first 21 ml of 1.6N HCl was utilized for matrix elution, while the following 25 ml was collected for pure Ca solution. Column chemistry typically exhibited yields exceeding 99%. To verify reproducibility and quality, each batch of column chemistry involved processing at least one reference material and blank as unknown samples. The overall procedural blank was less than 100 ng, which is insignificant relative to the 50 μg of Ca loaded onto the column.

Calcium isotope compositions were measured with thermal ionization mass-spectrometers (Thermo Triton) at two independent labs: State Key Laboratory of Isotope Geochemistry, Guangzhou Institute of Geochemistry (GIG), Chinese Academy of Sciences (CAS) and the State Key Laboratory of Oil and Gas Reservoir Geology and Exploitation, Chengdu University of Technology (CDUT). Both labs used the same Faraday cup setting on TIMS with ^{40}Ca, ^{41}K, ^{42}Ca, ^{43}Ca, and ^{44}Ca measured in static mode on the L2, C, H1, H2, and H3 cups, respectively. Each run consisted of sixteen blocks of thirteen cycles each, using an integration time of 4s. The ^{41}K was monitored to correct for ^{40}K interference on ^{40}Ca using $^{40}K/^{41}K = 1.7384 \times 10^{-3}$ (Heuser et al., 2002). Instrumental bias was corrected using the double-spike method by applying an iterative algorithm with the exponential law (Heuser et al., 2002). Calcium isotope compositions were reported relative to NIST SRM 915a using δ notation: $\delta^{44/40}Ca(‰) = 1000 \times [(^{44}Ca/^{40}Ca)_{sample}/(^{44}Ca/^{40}Ca)_{SRM\ 915a} - 1]$. Two standard deviations of $\delta^{44/40}$Ca in SRM915a measured throughout the course of this investigation is ±0.13‰ (N = 32), which represents long-term external precision. Duplicates of NWA 8336, NWA 2988, NWA 10079, and Millbillillie obtained by digestion of the two batches of powder were reproduced within the analytical error (Table 1). During the run, the $\delta^{44/40}$Ca for PCC-1 and BHVO-2 are 1.13 ± 0.06‰ (2SD, N = 3) and 0.82 ± 0.08‰ (2SD, N = 3), respectively, which are consistent with literature values (Table S1). Tatahouine was measured at both labs to test reproducibility and their results

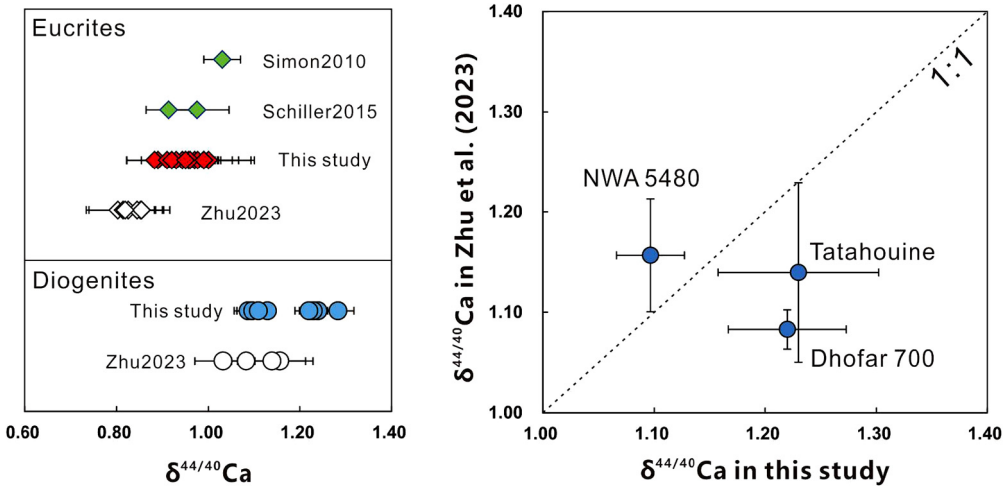

Fig. 2. Inter-lab Ca isotope data comparison. Data source: Simon and DePaolo (2010); Schiller et al. (2015); Zhu et al. (2023).

are consistent within analytical errors (1.19 ± 0.08‰ at CAS vs. 1.23 ± 0.07‰ at CDUT).

3. Results

3.1. Major and trace element compositions

Bulk rock element compositions are shown in Table S2 and Fig. 1. Most eucrites and diogenites show a limited variation in Mg content of 35-45.8 mg/g and 148-177 mg/g, respectively, falling into the range defined by literature monomict breccias (Fig. 1, Mittlefehldt, 2015 and references therein). The cumulate eucrite Dhofar 007 shows a higher Mg# (51.5) and a lower Ti content (1.86 mg/g) than basaltic eucrites. Eucrites and diogenites show a significant variation in trace element compositions. The monomict diogenites have La content from 25 to 225 ng/g and Lu from 11 to 41 ng/g. Basaltic eucrites have La content from 1960 to 6180 ng/g, Sc from 24.97 to 33.40 μg/g, and Hf from 0.75 to 2.09 μg/g. Polymict breccias (howardites NWA 10695 and NWA 8362, diogenite NWA 10079 and eucrite NWA 11704) show intermediate Ti, Mg, and Hf content between monomict eucrites and diogenites (Fig. 1). Notably, NWA 11055 is described as a polymict diogenite in the Meteoritical Society database, but its element compositions (Fig. 1) and Ca isotope compositions (Table 1) closely resemble the monomict eucrites. The lithology distribution in NWA 11055 may be heterogeneous and the investigated piece should be from a section that is mostly composed of eucritic clasts. Therefore, NWA 11055 is recognized as a monomict basaltic eucrite in the following discussion.

3.2. Calcium isotope compositions

Calcium isotope compositions are reported in Table 1. The basaltic eucrites show a homogeneous $\delta^{44/40}$Ca from 0.88 to 1.02‰ with an average of 0.95 ± 0.07‰ (2SD, N = 15), in agreement with the BSE estimate (0.94-1.05‰, Huang et al., 2010; Kang et al., 2017). The $\delta^{44/40}$Ca of cumulate eucrite Dhofar 700 (1.06 ± 0.09‰) is consistent with basaltic eucrites (0.95 ± 0.07‰). Diogenites show heavier Ca isotope compositions than eucrites with $\delta^{44/40}$Ca from 1.09 to 1.28‰ (on average of 1.18 ± 0.15‰). The polymict eucrite NWA 11704 (0.95 ± 0.09‰) and polymict diogenite NWA 11055 (0.95 ± 0.02‰) show consistent $\delta^{44/40}$Ca with monomict eucrites (0.88-1.00‰). Similarly, the polymict diogenite NWA 10079 has $\delta^{44/40}$Ca of 1.11 ± 0.09‰, overlapping the range of monomict diogenites (1.09 to 1.28‰). The two howardites NWA 10695 and NWA 8362 have Ca isotope compositions lighter than both eucrites and diogenites, with $\delta^{44/40}$Ca of 0.80 ± 0.08‰ and 0.86 ± 0.08‰, respectively.

4. Discussion

4.1. Mass-independent isotope variations in HED meteorites

^{40}Ca is one of two daughter products from the branched decay of ^{40}K (half-life 1.397 Ga, Steiger and Jäger, 1977). The measured $\delta^{44/40}$Ca can be decreased due to the ingrowth of ^{40}Ca, whose scale depends on the age and K/Ca ratio of samples. For instance, according to estimations in Fantle and Tipper (2014), samples with a K/Ca of 1 and an age of 1.0 Ga would have a 0.05‰ drop in $^{44/40}$Ca. Since diogenites have negligible K, their $\delta^{44/40}$Ca should not be affected. Eucrites have K concentrations ranging from 200 to 600 μg/g and K/Ca from 0.002 to 0.009 (Mittlefehldt, 2015). The average age of eucrites is 4.57 Ga (Hublet et al., 2017). Using the method in Fantle and Tipper (2014), the radiogenic ingrowth of ^{40}Ca is predicted to decrease the $\delta^{44/40}$Ca by 0.002 to 0.008‰ in eucrites, which is much smaller than the analytical uncertainty (±0.13‰). Huang and Jacobsen (2017) did not find measurable isotope anomaly on ^{40}Ca of eucrite Juvinas either. Therefore, the $\delta^{44/40}$Ca data of this study should not be affected by mass-independent Ca isotope variation.

4.2. Inter-lab data comparison

Stable calcium isotope compositions of HEDs have been measured by three different labs with different methods. Simon and DePaolo (2010) first reported eucrite Juvinas and diogenite Bilanga obtained by a ^{42}Ca-^{48}Ca double spike TIMS technique. Schiller et al. (2015) reported eucrite Juvinas and Stannern obtained by sample-standard bracketing MC-ICP-MS technique. Recently, Zhu et al. (2023) also used the sample-standard bracketing MC-ICP-MS technique on nine eucrites and four diogenites. Fig. 2 shows a comparison of our results with these studies. Our eucrites have $\delta^{44/40}$Ca of 0.95 ± 0.07‰ (2SD, N = 15), consistent with the Juvinas (0.98 to 1.03‰) and Stannern (0.91 ± 0.05‰) reported by Simon and DePaolo (2010) and Schiller et al. (2015). However, it shows that our eucrites are systematically heavier than those (0.83 ± 0.04‰) measured by Zhu et al. (2023). Three diogenites in this study (NWA 5480, Tatahouine, and Dhofar 700) were also analyzed by Zhu et al. (2023). Results of NWA 5480 are consistent for both studies (1.10 ± 0.03‰ for this study and 1.16 ± 0.06‰ for Zhu et al., 2023) but our Tatahouine (1.23 ± 0.07‰) and Dhofar 700 (1.22 ± 0.05‰) values are both higher than the results

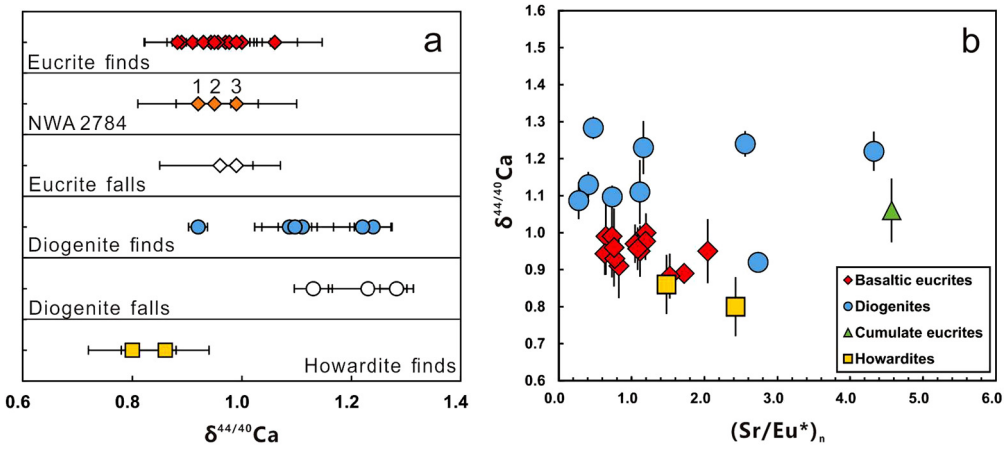

Fig. 3. (a) Comparison between the falls and the finds; and (b) $\delta^{44/40}$Ca vs. $(Sr/Eu^*)_n$.

(1.14 ± 0.09‰ and 1.08 ± 0.02‰, respectively) in Zhu et al. (2023). Zhu et al. (2023) argued that the TIMS data can be inaccurate for early formed meteorites due to radiogenic ingrowth ^{40}Ca. As we discussed in the previous section, this is not true for HEDs because of their extremely low K concentration (K_2O of BSV estimate is <0.01 wt.%, Righter and Drake, 1997). Although the reason for the systematically low $\delta^{44/40}$Ca in Zhu et al. (2023) is not clear, it possibly reflects sample heterogeneity or artificial bias. Nevertheless, the Ca isotope composition of HEDs needs further investigation. The following discussion only focuses on the new data in this study to avoid systematic uncertainty among different labs.

4.3. Terrestrial contamination

Although terrestrial weathering can significantly alter the chemical composition of HED meteorites (e.g., Barrat et al., 2010), there are several lines of evidence suggesting that weathering has a negligible Ca isotope effect in HEDs. (1) There is no systematic $\delta^{44/40}$Ca offset between the falls and the finds (Fig. 3a); (2) the altered minerals such as phosphates, sulfates, and carbonates will elevate the $(Sr/Eu^*)_n$ ratio (n denote chondrite normalized) in HEDs (Barrat et al., 2010). However, the $\delta^{44/40}$Ca shows no correlation with the $(Sr/Eu^*)_n$ ratio (Fig. 3b); and (3) the three duplicates of NWA 2784 were taken from different zones on the hand specimen. NWA 2784-1 was taken from the fusion crust and shows the highest degree of alteration. NWA 2784-2 was collected between the fusion crust and the fresh core with moderate alteration. NWA 2784-3 was sampled from the fresh core with minor alteration. These three fractions show an indistinguishable $\delta^{44/40}$Ca of 0.92 ± 0.11‰, 0.95 ± 0.03‰ and 0.99 ± 0.11‰, respectively (Fig. 3a). Therefore, the Ca isotope variations in HEDs should not reflect terrestrial weathering.

4.4. Calcium isotope composition of bulk silicate Vesta

The Ca isotope composition of BSV is a critical parameter as it provides a benchmark for differentiation of the internal and surface reservoirs for Vesta. The Vestan mantle is the largest geochemical reservoir for calcium, and the most reliable estimate for BSV should be based on observations of mantle rocks. However, the remote sensing of the Dawn spacecraft indicates that most HED meteorites sample the Vestan crust (Russell et al., 2012). Only a small number of Ol-bearing diogenites may represent mantle fragments (e.g., Tkalcec et al., 2013). This study measured one Ol diogenite NWA 5480. Tkalcec et al. (2013) observed the preferred orientation in Ol for NWA 5480 and attributed it to the solid-state plastic deformation that occurred in mantle conditions. However, whether NWA 5480 represents a mantle fragment of Vesta or not remains debated. Prior studies (Mitchell et al., 2021a; Yamaguchi et al., 2015) observed element zoning in Ol, Opx, and chromite in NWA 5480. In addition, Opx in NWA 5480 is fine grain size, which is contrary to the medium to coarse-grained Opx found in most diogenites. These signatures may reflect a rapid cooling event that occurred near the surface, suggesting that NWA 5480 represents an impact melt sheet instead of a mantle fragment. Therefore, NWA 5480 may not represent the composition of BSV. Eucrites are mantle-derived melts and may be used to investigate the Ca isotope composition of the Vestan interior. However, partial melting of a peridotite source can cause Ca isotope fractionation. For example, MORBs, generated by 10-20% partial melting of the terrestrial upper mantle, have Ca isotope compositions (~0.85‰) lighter than the BSE estimate (0.94-1.05‰). It is not known to what extent the eucrite represents the primary Vestan mantle.

Alternatively, the BSV can be estimated based on the characteristic of building blocks of Vesta. Nucleosynthetic isotope anomalies are effective tools in assessing the genetic relationships between meteorites and its planetary bodies. Several prior studies have revealed nucleosynthetic isotope dichotomy (e.g., ^{50}Ti and ^{54}Cr) between carbonaceous chondrites (CC) and non-carbonaceous chondrites (NC) (e.g., Kruijer et al., 2020). Such a signature has been interpreted to reflect the formation of meteorite parent bodies in the inner (NC) and the outer (CC) solar systems. Zhu et al. (2023) indicates that the inner solar system bodies may have heterogenous $\delta^{44/40}$Ca. However, the compilation of meteorite data in this study shows a contrasting conclusion. Within the NC group (Fig. 4), ordinary chondrites (OC) (0.97 ± 0.05‰, 2SE, N = 11), angrites (0.94 ± 0.0.08‰, N = 3), aubrites (0.97 ± 0.07‰, N = 6), bulk silicate Mars (1.04 ± 0.09‰ estimated by Magna et al., 2015), bulk silicate Moon (0.94 ± 0.03‰ estimated by Wu et al., 2020), and BSE (0.94-1.05‰ estimated by Huang et al., 2010; Kang et al., 2017) show a similar Ca isotope composition. Regarding enstatite chondrites (ECs), the pioneering study by Simon and DePaolo (2010) found that they have a systematically higher $\delta^{44/40}$Ca (1.16 to 1.51‰) than OCs. However, following studies (Amsellem et al., 2017; Huang and Jacobsen, 2017; Valdes et al., 2014) found no measurable Ca isotope variation between ECs (0.97 ± 0.04‰) and OCs (0.97 ± 0.05‰). Huang and Jacobsen (2017) indicated that the $\delta^{44/40}$Ca of the ECs in Simon and DePaolo (2010) may be affected by washing with water, which can dissolve oldhamite, the main Ca carrier in ECs. Thus, the Ca isotope composition of ECs should be similar to other NC groups. Notably, the two ureilites reported by Schiller et al. (2015) show heavier Ca isotope compositions (1.15 and 1.22‰, respectively) than OCs. This signature may reflect isotope fractionation during magmatic differentiation because ure-

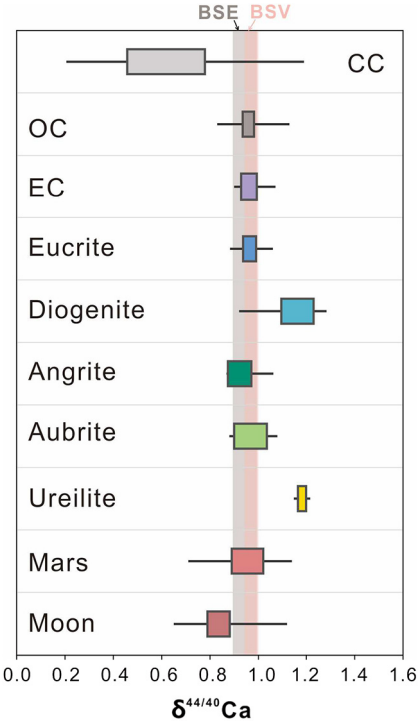

Fig. 4. Ca isotope compositions of chondrites, achondrites, lunar samples, and Martian meteorites. Boxes represent the spread of data around the median and error bars indicate outliers. The data source is from Valdes et al. (2021) and references therein. The gray and pink bars represent the BSE estimate (0.94 ± 0.05‰, Kang et al., 2017) and the BSV estimate of this study (0.97 ± 0.03‰), respectively. The ECs in Simon and DePaolo (2010) are not taken into consideration. The color version of this figure can be referred from the web version of this article.

ilites contain abundant olivine, which is isotopically heavier than other silicate minerals and melts (e.g., Xiao et al., 2022 and references therein). Nevertheless, it shows that most inner solar system bodies have a relatively homogeneous $\delta^{44/40}$Ca (0.97 ± 0.03‰, 2SE, N = 29, defined by the average of OCs, ECs, angrites and aubrites).

The ^{50}Ti and ^{54}Cr isotope anomalies reveal that HED meteorites fall within the field of NC groups, suggesting that Vesta should be accreted in the inner solar system (e.g., Kruijer et al., 2020). Therefore, we conclude that the $\delta^{44/40}$Ca of the BSV is 0.97 ± 0.03‰, similar to the average of inner solar system bodies (Fig. 4).

4.5. Calcium isotope compositions of basaltic eucrites: partial melting and magma ocean

It has been debated for decades whether the basaltic eucrites are remnant liquids of magma ocean differentiation (high melting degree, Greenwood et al., 2005; Mandler and Elkins-Tanton, 2013; Righter and Drake, 1997; Ruzicka et al., 1997) or are formed by partial melting of a primordial planetesimal (low melting degree, Mitchell et al., 2021b; Stolper, 1977). The homogenous oxygen isotope composition (e.g., Greenwood et al., 2005) and siderophile element signatures in basaltic eucrites (e.g., Co, Mo and W, McSween et al., 2010) favor extensive melting of Vesta, which forms a deep, global magma ocean. The magma ocean rapidly segregated and crystallized to yield a metallic core, Ol-rich mantle, Opx-rich lower crust, and basaltic upper crust. However, melting experiments conducted by Stolper (1977) show that some eucrites are saturated with pyroxene, Plg, Ol, metal, and spinel (Spl), indicating a origin of partial melting with degree <25%. Recently, MELTS modeling by Mitchell et al. (2021b) also suggested that eucrites should be generated by 15-20% partial melting of the primitive Vestan mantle.

Calcium isotopes can be fractionated during partial melting of a peridotitic source. Huang et al. (2010) first found that Opx in peridotite is isotopically heavier than the co-existing Cpx. Because Cpx is preferentially exhausted by melting compared to Opx and Ol, partial melts will be isotopically lighter than the refractory residue. This is consistent with observations on depleted peridotites (e.g., Kang et al., 2017) and MORBs (e.g., Eriksen and Jacobsen, 2022) that exhibit higher (+0.1-0.2‰) and slightly lower (−0.1‰) $\delta^{44/40}$Ca than the BSE estimate, respectively. The equilibrium Ca isotope fractionation value between mineral and melt ($\Delta^{44/40}Ca_{mineral\text{-}melt}$) is a key parameter to quantitatively evaluate the partial melting effect. Zhang et al. (2018) estimated the fractionation factors between melt and minerals (Cpx, Opx, and Plg) by first-principal calculation and ionic model. They conducted a peridotite melting simulation and indicated a negligible $\delta^{44/40}$Ca offset between partial melts (0.89-0.93‰) and BSE (0.94‰), which cannot explain the $\delta^{44/40}$Ca of MORB (~0.85‰). Notably, the simulation in Zhang et al. (2018) did not consider the Ca isotope effect of Ol. Although CaO in Ol (<0.1 wt.%) is lower than Cpx (~20 wt.%) and Opx (0.2-1 wt.%), its role in partial melting may not be neglected because Ol is isotopically heavier than the co-existing Cpx and Opx. Recently, Eriksen and Jacobsen (2022) and Soderman et al. (2022) used the fractionation factor of Ol, Opx, and Cpx reported by recent first-principal studies (e.g., Antonelli et al., 2019; Huang et al., 2019) to simulate the partial melting of peridotite. Their results indicate that the Ca isotope offset between partial melts and peridotite source should be larger than the predictions in Zhang et al. (2018) and can explain the Ca isotope composition of MORB.

We applied a similar model as Soderman et al. (2022) to constrain the partial melting of Vestan mantle. Since the mineral assemblage and the melting equations for Vestan pristine mantle remain unclear, we assume the lithology of Vestan pristine mantle similar to peridotite. KLB1 peridotite with a BSV-like $\delta^{44/40}$Ca, (a commonly used experimental composition as an analog for the upper terrestrial mantle; Davis et al., 2009), is used as the initial input. The melting is assumed to be isobaric with pressure anchored at 5 kbar and temperature is increased from 1373 K to 2123 K. The equilibrium Ca isotope fractionation factors are consistent with the values used in Soderman et al. (2022) and can be found in Table S3. Modeling results are presented in Fig. 5. The $\delta^{44/40}$Ca of partial melts varies from 0.86 to 0.93‰ at melting degree <20% and 0.88 to 1.00‰ at melting degree >20%. The 95% C.I. (i.e., confidence interval) of eucrite $\delta^{44/40}$Ca can be explained by >20% degree of partial melting. Therefore, Ca isotope signature indicates that eucrites can be formed by a moderate to high degree of partial melting of the pristine Vestan mantle.

Furthermore, we applied crystallization modeling to test the magma ocean hypothesis. Righter and Drake (1997) suggested that the early stage of Vestan magma ocean evolution should be by means of equilibrium crystallization because the efficient mixing of magma hampers the separation of crystalized minerals from melts. Mandler and Elkins-Tanton (2013) proposed a detailed magma ocean model that includes 60-70% equilibrium crystallization followed by continuously extraction of residual melt to shallow crustal magma chambers. Here, we used MELTs (Asimow and Ghiorso, 1998) to calculate Ca isotope evolution during magma ocean differentiation. The magma ocean is assumed to be generated by 100% melting of Vesta. The modeling invokes two scenarios: 60% and 70% equilibrium crystallization followed by fractional crystallization. The equilibrium crystallization modeling was run on the BSV composition estimated by Ashcroft and Wood (2015) from 1913 K downwards, decrementing the temperature by 1 K at each step. The fractional crystallization was run on the 60% or 70% melt composition predicted by the equilibrium crystallization model. The pressure was fixed at the atmospheric pressure. The

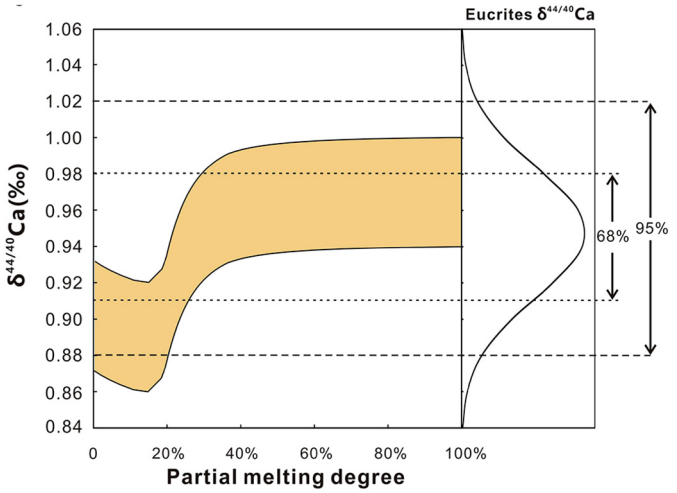

Fig. 5. Ca isotope composition of melt as a function of partial melting degree. The shaded area represents the predicted $\delta^{44/40}$Ca of melts. The BSV values is 0.97 ± 0.03‰ in this study. The right side of the figure shows the probability density distribution of eucrites $\delta^{44/40}$Ca. The dashed lines show the 68% and 95% C.I. by assuming that eucrite $\delta^{44/40}$Ca follow a Gaussian distribution.

isotope fractionation factors can be found in Table S3. Notably, Zhu et al. (2023) adopted 0.92 ± 0.11‰ as the bulk $\delta^{44/40}$Ca of the magma ocean, which is slightly heavier than their BSV estimate (0.83 ± 0.04‰). There is no clear reason why the magma ocean has a heavier Ca isotope composition than the BSV because (1) Ca isotopes cannot be fractionated by evaporation or metallic core separation during magma ocean differentiation; (2) residue minerals such as Ol and Opx are isotopically heavier than partial melts. Even if the magma ocean is generated by low degree partial melting, its bulk composition should be isotopically lighter than the BSV estimate.

The modeling results are presented in Fig. 6. The predicted crystallization sequence is similar to the results obtained by Mandler and Elkins-Tanton (2013), which can be roughly separated into four stages: (1) only Ol; (2) Ol + Opx; (3) Opx + Spl; (4) Cpx + Plg + Spl. Mandler and Elkins-Tanton (2013) indicated that basaltic eucrites may represent the residual melt of stage (4). Modeling shows that the magma ocean differentiation will not significantly alter the $\delta^{44/40}$Ca of residue melt. Most importantly, the calculated result of residue melts in stage (4) has consistent Ca isotope composition with basaltic eucrites measured in this study. Combined with the results from the melting model, the Ca isotope signature may indicate that basaltic eucrites represent the evolved melt of a magma ocean that is generated by a moderate to high degree of partial melting (>20%).

4.6. Calcium isotope variations in diogenites: crustal contamination

Within the magma ocean model (Fig. 6), diogenites represent the cumulates formed at stages (2) and (3) (e.g., Mandler and Elkins-Tanton, 2013; Righter and Drake, 1997). From this viewpoint, eucrites and diogenites had a common parental melt and were directly cogenetic. However, several studies found that the magma ocean model cannot explain the wide variations of trace elements in diogenites and thus argued that diogenites and eucrites are not necessarily related. Instead, they may be crystalized in multiple small magma chambers (e.g., Mandler and Elkins-Tanton, 2013) or formed by ultramafic melts that are derived from magma ocean cumulate intruding into the eucritic crust (e.g., Barrat et al., 2008, 2010; Mitchell and Tomkins, 2019). The intrusion model is further supported by Dawn's gravity data, which found high-density areas within the crust, and they may represent diogenitic intrusions (Ermakov et al., 2014).

Diogenites in this study show a variation of 0.3‰ in $\delta^{44/40}$Ca from 1.01 to 1.28‰. However, the $\delta^{44/40}$Ca of cumulates produced in stages (2) and (3) of magma ocean are expected to be >1.17‰ in either 60% or 70% equilibrium crystallization scenarios (Fig. 6). Therefore, diogenites in this study with $\delta^{44/40}$Ca < 1.17‰ may not be produced in the magma ocean stage and are not cogenetic with basaltic eucrites. This suggests that diogenites had a complex petrogenesis. The short-lived radioactive-isotope signatures also suggest diogenites do not share a common source. Schiller et al. (2017) showed that diogenites can be classified into two groups: (1) negative ^{26}Mg anomaly and little variability in Eu/Eu*; (2) positive ^{26}Mg anomaly and negative correlation between Eu/Eu* and ^{26}Mg anomaly. The former reflects cumulates derived from a thoroughly mixed magma ocean, while the latter should be produced in isolated magmatic systems.

The light Ca isotope composition (<1.17‰) of diogenites can be explained by crustal contamination. The $\delta^{44/40}$Ca of diogenites show a positive correlation with 1/Ca (Fig. 7a) and a negative correlation with the 1000 × Lu/Ti (Fig. 7b). The diverse concentrations of incompatible elements in diogenites have been attributed to the incorporation of trapped melt during crystallization (e.g., McSween et al., 2010) or assimilation of crustal melts (Barrat et al., 2010). Barrat (2004) argued that if trapped melt was added to the crystalized diogenite in the absence of plagioclase, the Eu/Eu* will increase. However, there is no correlation between $\delta^{44/40}$Ca and Eu/Eu* (Fig. 7c), indicating that the variations in $\delta^{44/40}$Ca cannot be attributed to the involvement of trapped melt. Alternatively, as eucrites have higher Lu/Ti and higher Ca content and lower $\delta^{44/40}$Ca than diogenites, the correlation observed in Fig. 7a and b can be explained by mixing between parental melt of diogenite and eucrite partial melts.

A mixing model is presented in Fig. 7b. The $\delta^{44/40}$Ca for the parental melt of diogenite is assumed to be from 1.17 to 1.32‰, similar to the composition of diogenites crystallized from the magma ocean. The 1000 × Lu/Ti ratio was assumed from 0.012 to 0.063 based on the diogenites in Barrat et al. (2008). The Ca isotope compositions and Lu and Ti contents of crustal partial melts are calculated by a batch melting model following the method in Barrat et al. (2007). The initial composition of eucrite used the Juvinas data in Barrat et al. (2007) and we calculated the partial melts compositions with 1%, 5%, 10% and 20% melting degree. Other parameters, including partition coefficients (D) and mineral abundance, are listed in Table S4 and modeling results are shown in Table S5.

The modeling results indicate that the 1000 × Lu/Ti ratio (0.063 to 0.068) and $\delta^{44/40}$Ca of melts (0.963 to 0.965‰) vary slightly with melting degree (1-20%). This is due to the similarity between bulk rock D_{Lu} (0.121) and D_{Ti} (0.106) and the low $\Delta^{44/40}Ca_{\text{bulk rock-melt}}$ (−0.02‰). Therefore, the 1000 × Lu/Ti ratio of eucrite melts end member is fixed at 0.068 and $\delta^{44/40}$Ca of 0.963‰. The modeling shows that the $\delta^{44/40}$Ca variation in diogenites can be explained by mixing with partial melts derived from the eucritic crust. In addition, our results suggest that the proportion of eucrite partial melts should be smaller than 10%, which is consistent with the conclusion in Barrat et al. (2010) based on the correlations between Eu/Eu* and Sm. Overall, the Ca isotope data in this study provide new evidence to show the complicated petrogenesis of diogenites. Samples with high $\delta^{44/40}$Ca (>1.17‰), low Lu/Ti, and low Ca content may be formed in the magma ocean stage, while the others with low $\delta^{44/40}$Ca (<1.17‰), high Lu/Ti, and high Ca content may be generated by magma ocean cumulate remelting and underwent subsequent intrusion-assimilation within the eucritic crust.

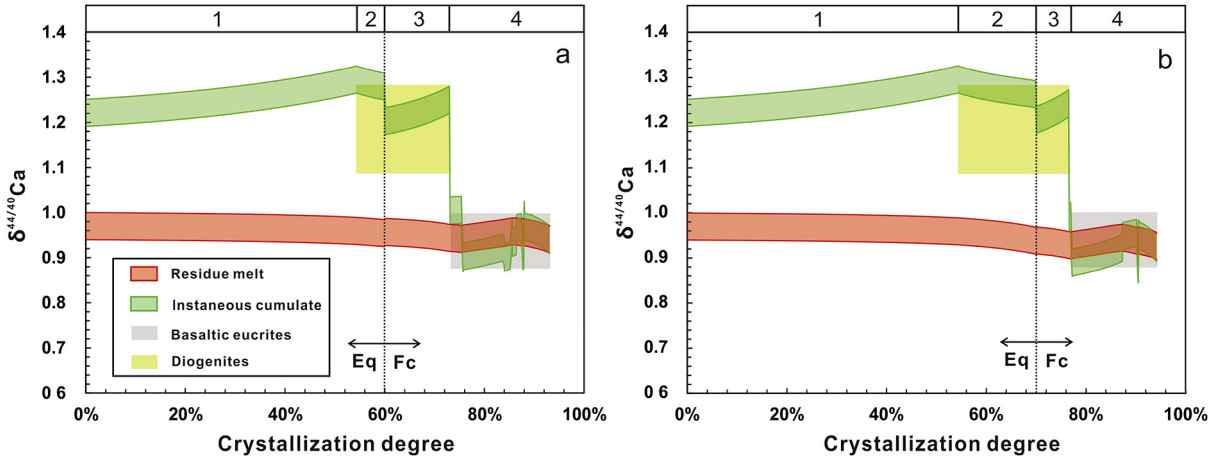

Fig. 6. The Ca isotope evolution of instaneous cumulate and residue melt during magma ocean differentiation by assuming 100% melting of proto-Vesta. The BSV value is 0.97 ± 0.03‰ in this study. Two scenarios were calculated: (a) 60% equilibrium crystallization (Eq) + 40% fractional crystallization (Fc); (b) 70% equilibrium crystallization +30% fractional crystallization. At the top of the figures is the crystallization sequence of Vesta magma ocean: (1) Ol; (2) Ol + Opx; (3) Opx + Spl; (4) Cpx + Plg + Spl.

4.7. Calcium isotope compositions of polymict breccias

The $\delta^{44/40}$Ca of two howardites, NWA 10695 (0.80 ± 0.04‰) and NWA 8362 (0.86 ± 0.05‰), are lower than both eucrites and diogenites (Fig. 3b and Table 1). Such a light isotope signature cannot be inherited from either eucritic or diogenitic clasts. Alternatively, it may reflect the signature of the impactor exogenous to Vesta. The addition of meteoritic materials in HEDs is characterized by the elevation of siderophile elements such as Ni because chondrites (1-1.7 wt.%, Wasson and Kallemeyn, 1988) and iron meteorites (5-17 wt.%, Haack and McCoy, 2003) have significantly higher Ni contents than HEDs (<30 μg/g). The two howardites in this study show high Ni content of 371 μg/g for NWA 8362 and 9822 μg/g for NWA 10695, indicating the incorporation of meteoritic material. The extraordinarily high Ni and other metal contents of NWA 10695 can be a manifestation for the incorporation of iron meteoritic material (see description for NWA 10695 on Meteoritical Society Database). Iron meteorites have no Ca and thus cannot affect the Ca isotope compositions of howardites, but most carbonaceous chondrites (Fig. 4) show lighter Ca isotope compositions than HEDs, which may explain the low $\delta^{44/40}$Ca of howardites.

We used a three-endmember mixing (diogenites, eucrites, and carbonaceous chondrites) to estimate the proportion of carbonaceous chondrites (Fig. 8). The chondrite-free sample is assumed to be a mixture with diogenite: eucrite ratio of 7:3. The chondrite endmember contains the compositions of CV, CR, and CM, which are the most abundant chondritic clasts in howardites (Warren et al., 2009). The modeling suggests that a 40-50% addition of carbonaceous chondrites is necessary to explain the $\delta^{44/40}$Ca of howardites. Despite the fact that some howardites can contain up to 60% chondrite fragments (Herrin et al., 2011), it is in contrast with the petrography observation that most howardites only contain a small percentage of chondritic materials (e.g., Zolensky et al., 1996). It may reflect that most chondritic materials melted during high-velocity impact. More studies are helpful for better understanding the Ca isotope composition of polymict breccia.

5. Conclusions

This study presents $\delta^{44/40}$Ca data on multiple varieties of HED meteorites, including basaltic eucrites (0.88-1.00‰), cumulate eucrite (1.06 ± 0.05‰), diogenites (0.92-1.28‰), and howardites (0.80-0.86‰). Due to the extremely low K concentration in HEDs, radiogenic ^{40}Ca ingrowth has a negligible effect on their $\delta^{44/40}$Ca. Falls and finds show no systematic Ca isotope offset and no correlation is observed between $\delta^{44/40}$Ca and $(Sr/Eu^*)_n$, suggesting that terrestrial weathering does not have obvious effect on Ca isotope composition of HED meteorites of this study.

Reported meteorite data show that inner solar system bodies have a homogeneous Ca isotope composition. The $\delta^{44/40}$Ca of BSV is estimated to be 0.97 ± 0.03‰ based on the average of OCs, ECs, angrite, and aubrite. Combined with partial melting and the magma differentiation model, eucrites can be explained as the evolved melts of a magma ocean that are generated by moderate to high degree partial melting (>20%) on primary Vesta.

Diogenites are generally heavier than basaltic eucrites and show ~0.3‰ $\delta^{44/40}$Ca variations. According to the magma ocean model, diogenites with $\delta^{44/40}$Ca<1.17‰ cannot be regarded as magma ocean cumulates. The $\delta^{44/40}$Ca of diogenites show a negative correlation with the 1000 × Lu/Ti ratio and a positive correlation with 1/Ca. This signature can be explained by magma-ocean-cumulate partial melts intruding into the eucritic crust and assimilating <10% crustal partial melts. Two howardites show lower $\delta^{44/40}$Ca (0.80-0.86‰) than both eucrites and diogenites, which may reflect the involvement of isotopically light chondritic materials. Overall, this study shows that Ca isotopes provide new insights into the formation of achondrites and the magmatic processes of the early solar system.

CRediT authorship contribution statement

YL Xue carried out the experiments. YL Xue and JT Kang analyzed data. JT Kang carried out the visualization, modeling, and wrote the initial manuscript. ZF Zhang, F Huang, and JT Kang designed the project and provided fund acquisition. SY Liao, RL Pang, BK Miao and WB Hsu provided samples and contributed to data interpretation. ZF Zhao and HM Yu helped with the analysis and data interpretation. All authors provided critical feedback and helped shape the manuscript.

Declaration of competing interest

The authors declare that they have no known competing financial interests or personal relationships that could have appeared to influence the work reported in this paper.

Data availability

Data will be made available on request.

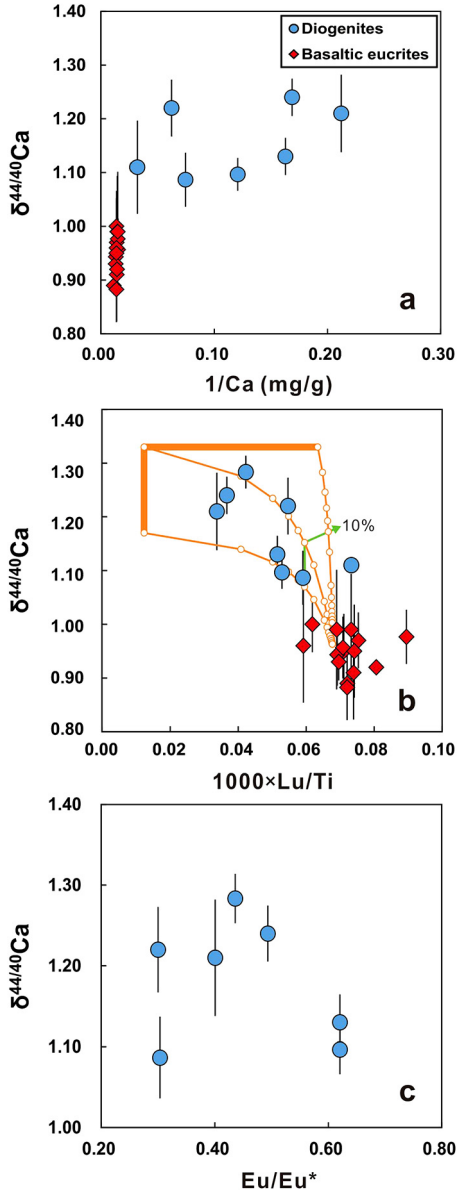

Fig. 7. (a) $\delta^{44/40}$Ca vs. 1/Ca (mg/g); (2) $\delta^{44/40}$Ca vs. 1000 × Lu/Ti; (3) $\delta^{44/40}$Ca vs. Eu/Eu*. The orange curves indicate mixing models between eucrite partial melts and diogenitic melts with varying compositions. The green arrow indicates 10% eucrite partial melts mixing with diogenitic melts.

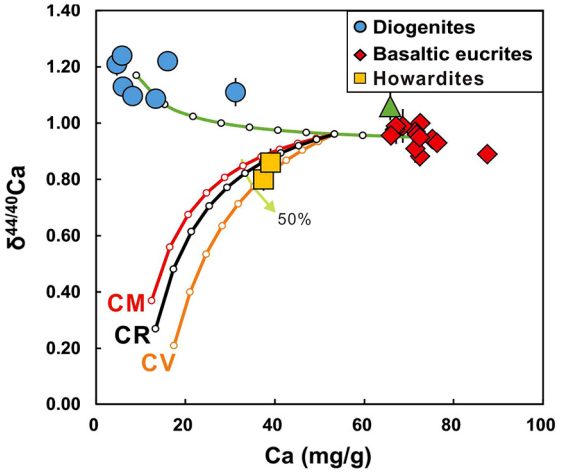

Fig. 8. Three-end member mixing between eucrite, diogenite, and chondrite (CM, CR and CV). Parameters used in calculations: diogenite: Ca = 9.1 mg/g and $\delta^{44/40}$Ca = 1.17‰; eucrite: Ca = 72.3 mg/g and $\delta^{44/40}$Ca = 0.95‰; CM: Ca = 12.5 mg/g (Braukmüller et al., 2018) and $\delta^{44/40}$Ca = 0.37‰ (Amsellem et al., 2017); CR: Ca = 13.4 mg/g (Braukmüller et al., 2018) and $\delta^{44/40}$Ca = 0.27‰ (Valdes et al., 2014); CV: Ca = 17.5 mg/g (Braukmüller et al., 2018) and $\delta^{44/40}$Ca = 0.21‰ (Amsellem et al., 2017).

Acknowledgements

We thank Fang Liu and Zhao Yan for their assistance with analysis. Part of the samples were provided by Xiaojia Zeng and Zhiqiang Shi. This work was supported by the Strategic Priority Research Program (B) of the Chinese Academy of Sciences (XDB41000000), the National Science Foundation of China (42241146, 42273007, 42203048, 42173022, 42073060, and 41873002), the China National Space Administration (CNSA) grant (D020202 and D020205), Scientific Research Starting Foundation of Wuzhou University (WZUQDJJ20095), and the Wuzhou University scientific research project (2021A005).

Appendix A. Supplementary material

Supplementary material related to this article can be found online at https://doi.org/10.1016/j.epsl.2023.118171.

References

Amsellem, E., Moynier, F., Pringle, E.A., Bouvier, A., Chen, H., Day, J.M., 2017. Testing the chondrule-rich accretion model for planetary embryos using calcium isotopes. Earth Planet. Sci. Lett. 469, 75–83.

Antonelli, M.A., Schiller, M., Schauble, E.A., Mittal, T., DePaolo, D.J., Chacko, T., Grew, E.S., Tripoli, B., 2019. Kinetic and equilibrium Ca isotope effects in high-T rocks and minerals. Earth Planet. Sci. Lett. 517, 71–82.

Ashcroft, H.O., Wood, B.J., 2015. An experimental study of partial melting and fractional crystallization on the HED parent body. Meteorit. Planet. Sci. 50, 1912–1924.

Asimow, P.D., Ghiorso, M.S., 1998. Algorithmic modifications extending MELTS to calculate subsolidus phase relations. Am. Mineral. 83, 1127–1132.

Barrat, J.A., 2004. Determination of parental magmas of HED cumulates: the effects of interstitial melts. Meteorit. Planet. Sci. 39, 1767–1779.

Barrat, J.A., Yamaguchi, A., Greenwood, R., Benoit, M., Cotten, J., Bohn, M., Franchi, I., 2008. Geochemistry of diogenites: still more diversity in their parental melts. Meteorit. Planet. Sci. 43, 1759–1775.

Barrat, J.A., Yamaguchi, A., Greenwood, R.C., Bohn, M., Cotten, J., Benoit, M., Franchi, I.A., 2007. The Stannern trend eucrites: contamination of main group eucritic magmas by crustal partial melts. Geochim. Cosmochim. Acta 71, 4108–4124.

Barrat, J.A., Yamaguchi, A., Zanda, B., Bollinger, C., Bohn, M., 2010. Relative chronology of crust formation on asteroid Vesta: insights from the geochemistry of diogenites. Geochim. Cosmochim. Acta 74, 6218–6231.

Braukmüller, N., Wombacher, F., Hezel, D.C., Escoube, R., Münker, C., 2018. The chemical composition of carbonaceous chondrites: implications for volatile element depletion, complementarity and alteration. Geochim. Cosmochim. Acta 239, 17–48.

Davis, F.A., Tangeman, J.A., Tenner, T.J., Hirschmann, M.M., 2009. The composition of KLB-1 peridotite. Am. Mineral. 94, 176–180.

Delaney, J.S., Takeda, H., Prinz, M., Nehru, C.E., Harlow, G.E., 1983. The nomenclature of polymict basaltic achondrites. Meteoritics 18, 103–111.

Eggins, S., Woodhead, J., Kinsley, L., Mortimer, G., Sylvester, P., McCulloch, M., Hergt, J., Handler, M., 1997. A simple method for the precise determination of≥ 40 trace elements in geological samples by ICPMS using enriched isotope internal standardisation. Chem. Geol. 134, 311–326.

Eriksen, Z., Jacobsen, S., 2022. Calcium isotope constraints on OIB and MORB petrogenesis: the importance of melt mixing. Earth Planet. Sci. Lett. 593, 117665.

Ermakov, A.I., Zuber, M.T., Smith, D.E., Raymond, C.A., Balmino, G., Fu, R.R., Ivanov, B.A., 2014. Constraints on Vesta's interior structure using gravity and shape models from the Dawn mission. Icarus 240, 146–160.

Fantle, M.S., Tipper, E.T., 2014. Calcium isotopes in the global biogeochemical Ca cycle: implications for development of a Ca isotope proxy. Earth-Sci. Rev. 129, 148–177.

Feng, C., Qin, T., Huang, S., Wu, Z., Huang, F., 2014. First-principles investigations of equilibrium calcium isotope fractionation between clinopyroxene and Ca-doped orthopyroxene. Geochim. Cosmochim. Acta 143, 132–142.

Gaffey, M.J., Bell, J.F., Cruikshank, D.P., 1989. Reflectance spectroscopy and asteroid surface mineralogy. J. Environ. Sci., 98–127.

Greenwood, R.C., Franchi, I.A., Jambon, A., Buchanan, P.C., 2005. Widespread magma oceans on asteroidal bodies in the early solar system. Nature 435, 916–918.

Haack, H., McCoy, T.J., 2003. Iron and stony-iron meteorites. In: Davis, A.M. (Ed.), Meteorites, Comets and Planets. In: Treatise on Geochemistry, vol. 1.
Herrin, J., Zolensky, M., Cartwright, J., Mittlefehldt, D., Ross, D., 2011. Carbonaceous chondrite-rich howardites; the potential for hydrous lithologies on the HED parent. In: 42nd Lunar and Planetary Science Conference.
Heuser, A., Eisenhauer, A., Gussone, N., Bock, B., Hansen, B., Nägler, T.F., 2002. Measurement of calcium isotopes (δ44Ca) using a multicollector TIMS technique. Int. J. Mass Spectrom. 220, 385–397.
Huang, F., Zhou, C., Wang, W., Kang, J., Wu, Z., 2019. First-principles calculations of equilibrium Ca isotope fractionation: implications for oldhamite formation and evolution of lunar magma ocean. Earth Planet. Sci. Lett. 510, 153–160.
Huang, S., Farkaš, J., Jacobsen, S.B., 2010. Calcium isotopic fractionation between clinopyroxene and orthopyroxene from mantle peridotites. Earth Planet. Sci. Lett. 292, 337–344.
Huang, S., Jacobsen, S.B., 2017. Calcium isotopic compositions of chondrites. Geochim. Cosmochim. Acta 201, 364–376.
Hublet, G., Debaille, V., Wimpenny, J., Yin, Q.Z., 2017. Differentiation and magmatic activity in Vesta evidenced by 26Al-26Mg dating in eucrites and diogenites. Geochim. Cosmochim. Acta 218, 73–97.
Kang, J., Ionov, D.A., Liu, F., Zhang, C., Golovin, A.V., Qin, L., Zhang, Z., Huang, F., 2017. Calcium isotopic fractionation in mantle peridotites by melting and metasomatism and Ca isotope composition of the Bulk Silicate Earth. Earth Planet. Sci. Lett. 474, 128–137.
Kruijer, T.S., Kleine, T., Borg, L.E., 2020. The great isotopic dichotomy of the early Solar System. Nat. Astron. 4, 32–40.
Li, B., Greig, A., Zhao, J., Collerson, K.D., Quan, K., Meng, Y., Ma, Z., 2005. ICP-MS trace element analysis of Song dynasty porcelains from Ding, Jiexiu and Guantai kilns, north China. J. Archaeol. Sci. 32, 251–259.
Lodders, K., 2003. Solar system abundances and condensation temperatures of the elements. Astrophys. J. 591, 1220.
Magna, T., Gussone, N., Mezger, K., 2015. The calcium isotope systematics of Mars. Earth Planet. Sci. Lett. 430, 86–94.
Mandler, B.E., Elkins-Tanton, L.T., 2013. The origin of eucrites, diogenites, and olivine diogenites: magma ocean crystallization and shallow magma chamber processes on Vesta. Meteorit. Planet. Sci. 48, 2333–2349.
McSween, H.Y., Mittlefehldt, D.W., Beck, A.W., Mayne, R.G., McCoy, T.J., 2010. HED meteorites and their relationship to the geology of Vesta and the Dawn mission. Space Sci. Rev. 163, 141–174.
Mitchell, J., Stephen, N., Tomkins, A., 2021a. Sampling an impact melt sheet with unusual diogenite northwest Africa 5480. In: LPI Contributions 2609, p. 6008.
Mitchell, J.T., Tomkins, A.G., 2019. On the source of diogenites and olivine diogenites: compositional diversity from variable fO2. Geochim. Cosmochim. Acta 258, 37–49.
Mitchell, J.T., Tomkins, A.G., Newton, C., Johnson, T.E., 2021b. A model for evolving crust on 4 Vesta through combined compositional and thermal modelling. Earth Planet. Sci. Lett. 571, 117105.
Mittlefehldt, D.W., 2015. Asteroid (4) Vesta: I. The howardite-eucrite-diogenite (HED) clan of meteorites. Geochemistry 75, 155–183.
Righter, K., Drake, M.J., 1997. A magma ocean on Vesta: core formation and petrogenesis of eucrites and diogenites. Meteorit. Planet. Sci. 32, 929–944.
Russell, C.T., Raymond, C.A., Coradini, A., McSween, H.Y., Zuber, M.T., Nathues, A., De Sanctis, M.C., Jaumann, R., Konopliv, A.S., Preusker, F., Asmar, S.W., Park, R.S., Gaskell, R., Keller, H.U., Mottola, S., Roatsch, T., Scully, J.E.C., Smith, D.E., Tricarico, P., Toplis, M.J., Christensen, U.R., Feldman, W.C., Lawrence, D.J., McCoy, T.J., Prettyman, T.H., Reedy, R.C., Sykes, M.E., Titus, T.N., 2012. Dawn at Vesta: testing the protoplanetary paradigm. Science 336, 684–686.
Ruzicka, A., Snyder, G.A., Taylor, L.A., 1997. Vesta as the howardite, eucrite and diogenite parent body: implications for the size of a core and for large-scale differentiation. Meteorit. Planet. Sci. 32, 825–840.
Schiller, M., Connelly, J.N., Bizzarro, M., 2017. Lead and Mg isotopic age constraints on the evolution of the HED parent body. Meteorit. Planet. Sci. 52, 1233–1243.
Schiller, M., Paton, C., Bizzarro, M., 2015. Evidence for nucleosynthetic enrichment of the protosolar molecular cloud core by multiple supernova events. Geochim. Cosmochim. Acta 149, 88–102.
Simon, J.I., DePaolo, D.J., 2010. Stable calcium isotopic composition of meteorites and rocky planets. Earth Planet. Sci. Lett. 289, 457–466.
Soderman, C.R., Shorttle, O., Matthews, S., Williams, H.M., 2022. Global trends in novel stable isotopes in basalts: theory and observations. Geochim. Cosmochim. Acta 318, 388–414.
Steiger, R.H., Jäger, E., 1977. Subcommission on geochronology: convention on the use of decay constants in geo- and cosmochronology. Earth Planet. Sci. Lett. 36, 359–362.
Stolper, E., 1977. Experimental petrology of eucritic meteorites. Geochim. Cosmochim. Acta 41, 587–611.
Tkalcec, B.J., Golabek, G.J., Brenker, F.E., 2013. Solid-state plastic deformation in the dynamic interior of a differentiated asteroid. Nat. Geosci. 6, 93–97.
Valdes, M.C., Bermingham, K.R., Huang, S., Simon, J.I., 2021. Calcium isotope cosmochemistry. Chem. Geol. 581, 120396.
Valdes, M.C., Moreira, M., Foriel, J., Moynier, F., 2014. The nature of Earth's building blocks as revealed by calcium isotopes. Earth Planet. Sci. Lett. 394, 135–145.
Wang, W., Zhou, C., Qin, T., Kang, J., Huang, S., Wu, Z., Huang, F., 2017. Effect of Ca content on equilibrium Ca isotope fractionation between orthopyroxene and clinopyroxene. Geochim. Cosmochim. Acta 219, 44–56.
Warren, P.H., Kallemeyn, G.W., Huber, H., Ulff-Møller, F., Choe, W., 2009. Siderophile and other geochemical constraints on mixing relationships among HED-meteoritic breccias. Geochim. Cosmochim. Acta 73, 5918–5943.
Wasson, J.T., Kallemeyn, G.W., 1988. Compositions of chondrites. Philos. Trans. R. Soc. Lond. Ser. A, Math. Phys. Sci. 325, 535–544.
Wu, W., Xu, Y., Zhang, Z., Li, X., 2020. Calcium isotopic composition of the lunar crust, mantle, and bulk silicate Moon: a preliminary study. Geochim. Cosmochim. Acta 270, 313–324.
Xiao, Z., Zhou, C., Kang, J., Wu, Z., Huang, F., 2022. The factors controlling equilibrium inter-mineral Ca isotope fractionation: insights from first-principles calculations. Geochim. Cosmochim. Acta 333, 373–389.
Yamaguchi, A., Barrat, J.A., Shirai, N., Ebihara, M., 2015. Petrology and geochemistry of Northwest Africa 5480 diogenite and evidence for a basin-forming event on Vesta. Meteorit. Planet. Sci. 50, 1260–1270.
Zhang, A.C., Kawasaki, N., Bao, H., Liu, J., Qin, L., Kuroda, M., Gao, J.F., Chen, L.H., He, Y., Sakamoto, N., Yurimoto, H., 2020. Evidence of metasomatism in the interior of Vesta. Nat. Commun. 11, 1289.
Zhang, H., Wang, Y., He, Y., Teng, F.Z., Jacobsen, S.B., Helz, R.T., Marsh, B.D., Huang, S., 2018. No measurable calcium isotopic fractionation during crystallization of Kilauea Iki lava lake. Geochem. Geophys. Geosyst. 19, 3128–3139.
Zhu, H., Zhang, Z.F., Wang, G.Q., Liu, Y.F., Liu, F., Li, X., Sun, W.D., 2016. Calcium isotopic fractionation during ion-exchange column chemistry and thermal ionisation mass spectrometry (TIMS) determination. Geostand. Geoanal. Res. 40, 185–194.
Zhu, K., Hui, H., Klaver, M., Li, S.-J., Chen, L., Hsu, W., 2023. Calcium isotope evolution during differentiation of Vesta and calcium isotopic heterogeneities in the inner solar system. Geophys. Res. Lett. 50, e2022GL102179.
Zolensky, M.E., Weisberg, M.K., Buchanan, P.C., Mittlefehldt, D.W., 1996. Mineralogy of carbonaceous chondrite clasts in HED achondrites and the Moon. Meteorit. Planet. Sci. 31, 518–537.